Earth and Planetary Science Letters 296 (2010) 469–480

Contents lists available at ScienceDirect

Earth and Planetary Science Letters

journal homepage: www.elsevier.com/locate/epsl

The early formation of the IVA iron meteorite parent body

Janne Blichert-Toft [a,*], Frédéric Moynier [b], Cin-Ty A. Lee [c], Philippe Telouk [a], Francis Albarède [a]

[a] Ecole Normale Supérieure de Lyon, Université Claude Bernard-Lyon I and CNRS, 69007 Lyon, France
[b] Washington University and McDonnell Center for Space Sciences, St Louis, MO 63130, USA
[c] Rice University, Houston, TX 77005, USA

ARTICLE INFO

Article history:
Received 11 April 2010
Received in revised form 24 May 2010
Accepted 28 May 2010
Available online 22 June 2010

Editor: T. Spohn

Keywords:
Pb isotopes
W isotopes
chronology
absolute age
IVA iron meteorites
troilite
cooling rate
early Solar System
least-square

ABSTRACT

The IVA iron meteorites are magmatic cumulates from the core of a small asteroid, which broke apart ~400 Ma ago. As the depletion of this planetary body in volatile elements is expected to be reflected in high U/Pb ratios of its minerals, we embarked on analyzing the isotope composition of Pb in the cm-sized troilite inclusions of Muonionalusta and Gibeon, both iron meteorites belonging to the IVA family. The bulk of the data for nine troilite subsamples of Muonionalusta scatter with an apparent age of 4.57 Ga, which is shown to reflect the presence of both primordial and common terrestrial Pb components, in addition to radiogenic Pb. The most radiogenic subsample, however, has fractions with $^{206}Pb/^{204}Pb$ ratios as high as over 1000 and gives a statistically significant $^{207}Pb^*/^{206}Pb^*$ age of 4565.3 ± 0.1 Ma (MSWD = 0.08), consistent with the ^{182}Hf–^{182}W metal–silicate segregation age of 2.4 ± 2.0 Ma. These data make the age of Muonionalusta the oldest documented yet for all differentiated bodies in the Solar System and constitute the first high-precision Pb–Pb age determined for crystallization of a phase contained within an iron meteorite group, hence advancing our understanding of early Solar System chronology. Using literature values for the cooling rate, and assuming a closure temperature for Pb of 300 °C, it is further estimated that the IVA parent body accreted within 1 Ma of CAI formation and had cooled to the Pb closure temperature within an additional 1–2 Ma. The overlap between the high-precision Pb–Pb and Hf–W ages points to a small, or rapidly fragmented, planetary body. The isotopic composition of Pb in Gibeon troilite yields a significantly younger age of 4544 ± 7 Ma (MSWD = 1.5), consistent with evidence from the ^{107}Pd–^{107}Ag chronometer, but we believe this age has been reset by melting upon shock. One puzzling observation is that the apparent $^{232}Th/^{238}U$ of Muonionalusta troilite is particularly low (~0.32), requiring a mechanism capable of efficiently fractionating Th from U, presumably the reduction of U to its trivalent form or the crystallization of phosphate. Average Pb concentrations of the order of 5–10 ppb and high $^{238}U/^{204}Pb$ ratios of >1000 require U concentrations in troilite in the sub-ppb to one ppb range. This may indicate that troilite inclusions in IVA meteorites do not represent metal-sulfide unmixing, but rather correspond to late-stage S-rich liquid residues from extreme crystallization of the interstitial melts.

1. Introduction

Observations and measurements made on meteorites offer rare clues about the numerous processes taking place during the first few million years of the history of the Solar System. Isotopic measurements in particular shed light on the chronology of these processes. Over the last several decades, the assumption that iron meteorites likely formed in bodies with lengthy accretionary histories and protracted periods of differentiation and crystallization has gradually given way to accumulating isotopic evidence that the crystallization of at least some of these bodies occurred within a very few million years of the start of the Solar System (Chen and Wasserburg, 1990; Horan et al., 1998; Lee, 2005; Markowski et al., 2006; Scherstén et al., 2006; Qin et al., 2008; Schönbächler et al., 2008). The emerging testimony for the rapid progression of early planetary processes requires that some iron meteorites were extracted from small, very early-formed asteroids. The nature of these bodies and their evolution in the rapidly evolving solar nebula are not well understood. Although the debris disk left by accretion of planetary bodies from the solar nebula appears to have dissipated in less than a few Ma (Wyatt, 2008), firsthand records of old ages in planetary objects are scarce, mostly because radiometric ages reflect cooling ages, while heating by the radioactive decay of ^{26}Al, tidal dissipation, and repeated impacts were keeping planetary interiors hot. Exceptions exist, such as the angrite d'Orbigny with a documented Pb–Pb age of 4564.4 Ma (Amelin, 2008). Core segregation within the parent asteroids of at least some iron meteorites seems to have started very early, but has been variably dated depending on which chronometer is considered. Presumably, ^{187}Re–^{187}Os (Horan et al., 1998) and ^{107}Pd–^{107}Ag (Chen and Wasserburg, 1990; Schönbächler et al., 2008) ages are those of

* Corresponding author. Tel.: +33 (0)4 72 72 84 88.
E-mail address: jblicher@ens-lyon.fr (J. Blichert-Toft).

0012-821X/$ – see front matter © 2010 Elsevier B.V. All rights reserved.
doi:10.1016/j.epsl.2010.05.036

metal crystallization or subsolidus closure, whereas ^{182}Hf–^{182}W (Horan et al., 1998; Lee, 2005; Markowski et al., 2006; Scherstén et al., 2006; Qin et al., 2008) dates silicate–metal segregation. The latter chronometer in particular strongly suggests that iron meteorites are very old differentiated objects that formed within only a few Ma of Allende CAIs. However, the limiting precision on W and Ag ages of, respectively, ~2 and ~4 Ma, and the current range of 1.6 Ma on the age of CAIs used to anchor both the ^{182}Hf–^{182}W and ^{107}Pd–^{107}Ag chronometers, stand in the way of finding out precisely how old.

Although some iron meteorites, such as, most famously, Canyon Diablo, have been found to contain the least radiogenic (i.e., primitive or primordial) Pb in the Solar System (Patterson, 1956; Tatsumoto et al., 1973; Chen and Wasserburg, 1983; Göpel et al., 1985), others contain Pb radiogenic enough to allow for an investigation into their chronological potential in terms of absolute ages (Chen and Wasserburg, 1983), which is why we set out to date some of these objects using the Pb–Pb chronometers. The ^{207}Pb/^{206}Pb chronometer has the unique property that ages are independent of measured parent/daughter ratios and, therefore, largely insensitive to recent resetting. In addition, and contrary to extinct radioactivities, the ^{207}Pb/^{206}Pb chronometer defines an absolute time scale that renders it independent of CAI age constraints. In fact, it is the ^{207}Pb/^{206}Pb chronometer itself which is used to date the CAIs in the first place (Bouvier et al., 2007; Amelin and Krot, 2007; Connelly et al., 2008; Jacobsen et al., 2008; Wadhwa and Bouvier, 2009). The final advantage of the ^{207}Pb/^{206}Pb chronometer is its remarkable precision (due to the combination of a short-lived, almost extinct (^{235}U) and a long-lived (^{238}U) parent nuclide and the parent element being common to both chronometers), potentially better than 1 Ma, even for ages as old as that of the Solar System.

Among the magmatic iron meteorites, the IVA group is known to be depleted in volatiles, such as Ga and Ge (Wasson and Richardson, 2001). This group is not, however, adequately accounted for by a simple fractional crystallization model with a unique initial S content (Chabot, 2004). The IVA group is also known for its broad and somewhat controversial range of cooling rates, between 30 and 6600 K per Ma (Rasmussen et al., 1995; Haack et al., 1996; Wasson and Richardson, 2001; Yang et al., 2007, 2008), which has been interpreted as the disruption and reassembly of the core of an early planet 5–200 km in diameter. Low-Ni members of this group may have cooled down as fast as 1500 K Ma^{-1}. Oxygen isotopes suggest that the IVA irons and the L and LL ordinary chondrites may have been extracted from the same parent body (Wang et al., 2004). Because of its large range in Pd/Ag ratios, Gibeon, which belongs to the IVA group, has become the reference for ^{107}Pd–^{107}Ag ages (Chen and Wasserburg, 1990; Schönbächler et al., 2008). Muonionalusta is another, but less well known member of the IVA group, with large fragments excavated in Sweden from north of the Arctic Circle. It is an octahedrite that contains large, cm-sized inclusions of troilite (Lagerbäck and Wickman, 1997). The presence of stishovite signifies that this meteorite was heavily shocked, possibly during the 0.4 Ga old breakup event indicated by cosmic ray exposure (Voshage, 1967; Lavielle et al., 1999) and the associated shower (Holtstam et al., 2003). The Pb–Pb dating of troilite inclusions from two separate samples of Muonionalusta and the implications of their ages for the early history of the Solar System is the main focus of the present work, although we also show Pb–Pb isotope data for a troilite inclusion from Gibeon, and Hf–W isotope data for Muonionalusta iron.

2. Samples and analytical techniques

Two large samples of Muonionalusta (thin slabs, one rectangular and one triangular, of ~350 g each measuring, respectively, 8×10×0.7 cm and 12×14×15×0.3 cm) were acquired from an anonymous German meteorite dealer (the rectangular slab hereafter referred to as ML1) and from Luc Labenne, a French meteorite dealer (the triangular slab hereafter referred to as ML2). Each slab contained a single large troilite inclusion, one only slightly elongated, the other ellipsoidal, with dimensions of about 3.5×2×0.7 cm (ML1) and 6×3×0.3 cm (ML2). The following sample characteristics are largely reproduced from the descriptions by Buchwald (1975) and Holtstam et al. (2003) of different pieces of Muonionalusta. The iron shows a fine Widmanstätten pattern with long kamacite lamellae. Wasson and Richardson (2001) reported an average Ni content of the iron of 8.48 wt.%. Troilite varies from schreibersite, with the composition of $Fe_{0.97}Cr_{0.02}S$, to kamacite near the edge, with the composition of $Fe_{1.56}Ni_{1.44}P$. The troilite is accompanied by subhedral grains of chromite, elongated grains of daubreelite ($Fe^{2+}Cr_2S_4$), and rare stishovite, all up to 100 μm long.

A 120 g piece of Gibeon in the form of a thick slab measuring 5×4×1.2 cm with half of a single large, nearly circular (3.5×3×1.2 cm) troilite inclusion comprising about a third of the iron meteorite sample also was obtained from Luc Labenne. The troilite inclusion itself contained small (~0.5 cm) spherical metal blebs scattered within the sulfide matrix with a conspicuous metal-sulfide eutectic rim. From the detailed petrological descriptions given by Buchwald (1975) and Teshima et al. (1986), the two meteorites, Muonionalusta and Gibeon, and their troilite inclusions, are similar, with the sole difference that stishovite has not been found in Gibeon troilite. Teshima et al. (1986) argued that Gibeon underwent some event of flash heating followed by rapid cooling. Wasson and Richardson (2001) report a range of Ni content in the metal of 7.9–8.2 wt.%.

Several troilite subsamples (nine for Muonionalusta and one from Gibeon) in the form of massive chunks (1.6–3.5 g) were extracted from the troilite inclusions of the two slabs of Muonionalusta and the single slab of Gibeon using a stainless steel chisel. One of the Muonionalusta subsamples and the Gibeon sample were first analyzed on an Element 2 LA-ICP-MS at Rice University to verify their true troilite nature and determine their depletion levels for Pb, U, and Th. As expected, high concentrations of Fe, S, Cr, and Ni (of the order of wt.%), as well as Mn, Co, Cu, P, and Zn (of the order of ppm), and very low concentrations of Pb, U, and Th (of the order of ppt to ppb) were found (Table 1). The laser ablation measurements were done on a ThermoFinnigan Element 2 single-collector magnetic sector ICP-MS using a 213 nm New Wave laser. Samples were ablated with an energy flux of 16–18 J/cm^2 at a 10 Hz repetition rate. Spot diameters varied from 55 to 110 μm. ^{57}Fe, ^{60}Ni, ^{33}S, ^{52}Cr, ^{59}Co, ^{31}P, ^{55}Mn, ^{63}Cu, and ^{66}Zn were determined in medium mass resolution mode (m/Δm ~3000), which was sufficient to resolve all relevant

Table 1
Major and trace element abundances in Muonionalusta and Gibeon troilites.

Sample	Muonionalusta all (n=21)		Muonionalusta[a] (n=14)		Gibeon (n=4)	
	Mean	2s	Mean	2s	Mean	2s
Fe (wt.%)	59.2	7.78	60.2	7.6	58.3	2.88
S (wt.%)	40.1	6.43	39.6	7.6	41.4	2.83
Cr (wt.%)	0.264	0.0357	0.26	0.039	0.246	0.0381
Ni (wt.%)	0.326	0.755	0.0294	0.00558	0.0238	0.0041
Mn (ppm)	300	81	300	55	350	260
Cu(ppm)	200	190	170	130	110	51
Co (ppm)	630	660	22	11	16	8.7
P (ppm)	170	800	5.2	3.6	380	740
Zn (ppm)	1.4	3.5	0.78	0.56	66	150
Pb (ppm)	0.04	0.29	0.0077	0.0074	0.097	0.24
Th (ppm)	0.0014	0.0035	0.0019	0.0042	0.00054	0.00024
U (ppm)	0.0015	0.0078	0.00081	0.0038	0.0028	0.0044

[a] Homogeneous domain within the same inclusion (n = number of analyses; 2s = 2 sigma).

isobaric interferences. ^{57}Fe, ^{60}Ni, ^{55}Mn, ^{52}Cr, ^{59}Co, ^{238}U, ^{232}Th, and ^{208}Pb were determined in low mass resolution mode (m/Δm ~ 300). Long-term magnetic drift in medium mass resolution was corrected for during every run by centering on the ^{40}Ar^{40}Ar dimer. Hysteresis effects in medium mass resolution mode were accounted for by applying specific offsets to each mass analyzed. These effects were not important for the low mass resolution mode. The Hoba and Filomena iron meteorites were used as external standards for Fe, Ni, Co, P, and Cu (Campbell et al., 2002), stoichiometric pyrite was used for Fe and S, and two USGS basaltic glass standards (BHVO-2g and BCR-2g) were used for Fe, Mn, Co, P, Cu, Zn, Cr, U, Th, and Pb (GEOREM). During analysis, a gas background of ~10 slices was acquired (~40 s), followed by ~40 slices taken during ablation (~160 s). Gas backgrounds were subtracted from sample signals. These background-corrected analyses were then normalized to ^{57}Fe. Calibration curves were based on multiple standards when possible. In particular, ^{57}Fe-normalized signals for Co, Ni, and Cu in the silicate glass and iron meteorite standards were collinear, indicating no significant matrix effects between metals and silicates.

All the Muonionalusta samples and the Gibeon sample were then repeatedly leached in 0.5 N and 1 N HNO_3, 8 N or 50% HF, and one sample also in concentrated HCl, while Gibeon was leached successively simply in 1 N, 2.5 N, and 7 N HNO_3 having established from the previous leaching experiments on Muonionalusta that HF dissolves unwanted silicate inclusions, potentially compromised by terrestrial contamination, HCl is completely inefficient for Pb, while stronger HNO_3 is more effective than dilute HNO_3 at leaching out Pb. The resulting residues finally were dissolved in concentrated HNO_3. Next, for some of the samples (not all, see Table 2, as this step was added to the Pb purification protocol only after a first set of samples had already been processed and analyzed), the dried-down leachates and residues were redissolved in 8 N HCl in order to extract their Fe contents into fresh isopropylether (Dodson et al., 1936; Myers and Metzler, 1950), which had first been purified for any trace amounts of contaminant Pb by several back-extractions into dilute HCl. The Fe-extraction step, which was done twice in order to achieve complete extraction (98% of Fe was found to be extracted during the first step), was undertaken in order to facilitate subsequent Pb elution and optimize Pb yields, which were essentially 100%. Lead for all the leachates and residues was separated from the FeS- or, when Fe had been extracted, the S-dominated matrix on 150 μl anion-exchange (AG1-X8, 200–400 mesh) teflon columns using 1 N HBr and 6 N HCl. All samples were run through the Pb columns twice to ensure the cleanest possible Pb for isotope analysis. Double-distilled reagents were used throughout for all sample leaching, dissolution, Fe solvent extraction, and column elution procedures.

The purified Pb was analyzed for its isotopic composition on the Nu Plasma 500 HR multiple-collector inductively-coupled plasma mass spectrometer (MC-ICP-MS) at the Ecole Normale Supérieure (ENS) in Lyon using standard bracketing (the NIST 981 Pb standard was run systematically every two samples) and Tl to monitor instrumental mass bias and correct for mass fractionation. We used the triple-spike values of Eisele et al. (2003) for normalization to the NIST 981 Pb standard (see Albarède et al., 2004, for details). Typical internal uncertainties on the Pb isotopic ratios were about 50–100 ppm. The amounts of Pb analyzed for each leachate and residue are provided in Table 2 and correspond to the sample signal intensities calibrated with respect to the intensity of the Pb ion beam signal obtained for the 35 ppb NIST 981 Pb standard solution run in alternation with the samples. These leachate and residue concentrations, when added together for each troilite subsample and divided by the sample weight and subtracting what is clearly excess contaminant Pb for some of the first leachates, correspond well with the average Pb concentrations obtained by LA-ICP-MS on the bulk troilite. Total procedural Pb blanks were estimated in two different ways: first by running a complete chemistry without any sample added (15 pg), and, second, by assuming that the smallest sample analyzed in this project (sample ML2-sa2-L4-N1, Table 2) only contains radiogenic and contaminant Pb (<40 pg).

The average and 2-sigma values of Tl-normalized isotope compositions of 82 NIST 981 standards run during the course of this study (eight 18-hour run sessions over one year) are listed in Table 3 together with the triple-spike values of Eisele et al. (2003). The quoted precision on our standard measurements does not take sample-standard (S/S) bracketing into account, which, upon application, improves the precision on the samples by a further factor of 3–5 over the simple Tl normalization shown in Table 3.

Although the washes from the Pb columns were collected in clean beakers for the purpose of later separating U for isotopic analysis, we did not obtain enough U to measure statistically significant U isotope compositions. We ignore if this is due to the only tiny amounts of U in the troilite (calculated from the Pb ion beam signals and the apparent μ values of the samples after blank correction, Table 2), to U being withheld by some refractory phase left undissolved because of not using high-pressure bombs for the dissolution procedure (a choice made intentionally to avoid the significantly higher Pb blanks of PTFE bombs; see Bouvier et al., 2007, for details), or to interference of sulfur in the form of sulfate from the S-heavy sample matrix on the U columns leading to partial loss of U during the elution procedure (for which both standard anion-exchange, Eichrom UTEVA, and LN-Spec resins were tried in conjunction with 3 N HNO_3 and 0.05 N HCl:0.3 N HF, including using ascorbic acid to reduce the sulfate). However, even if we had been successful in collecting all of the U, then for 0.1 ng of U, which is the order of magnitude of U in our leachates, the predicted 2-sigma uncertainty from counting statistics on ^{238}U/^{235}U for such a small amount, assuming an ion yield on the mass spectrometer of 0.1%, would be 137.8 ± 0.2, a range that covers most of the variation observed by (Brennecka et al. (2010a)) in CAIs, and, hence, neither informative nor conclusive.

Measurement errors for Pb isotope compositions are either the 2-sigma relative in-run errors or the standard reproducibility, whichever is greater. Data uncertainties were calculated by Monte-Carlo error propagation assuming a Pb isotope composition of the blank of ^{206}Pb/^{204}Pb = 18.35, ^{207}Pb/^{206}Pb = 0.8549, and ^{208}Pb/^{206}Pb = 2.085, with errors of 2, 0.4, and 0.4%, respectively, and a blank of 15 pg supposed to be known to within a factor of two. The details of these calculations can be found in Bouvier et al. (2007).

The chemical separation and mass spectrometry techniques used for W are summarized in Moynier et al. (2009). Iron fragments from ML1 and ML2 of ~1 g each were first cleaned in distilled water for 5 min in an ultrasonic bath. After removal of the leaching solution, the samples were dissolved in a mixture of concentrated HNO_3 and HCl. The metal went readily into solution within a few hours. Tungsten was then separated from the matrix on an anion-exchange column using the procedure described in Irisawa and Hirata (2006). In order to completely remove Os, which interferes isobarically with W during mass spectrometric analysis, concentrated HNO_3 was added to the sample several times and heated to drive off volatile Os. The average sample yields for W were >90% and the total procedural W blank ~0.9 ng, the latter being a direct result of the high W yields aimed at for the present W elution protocol, but still negligible compared to the elevated W contents of iron meteorites of >1 μg.

The W isotope compositions were measured on the large geometry high mass resolution Nu Plasma 1700 MC-ICP-MS at ENS Lyon. Potential isobaric interferences from Os on the W masses 184 and 186 were monitored by measuring the intensity of ^{188}Os, but were negligible for the present samples due to the repeated treatment of the samples during chemical processing with boiling concentrated HNO_3. An exponential law was used to correct for instrumental mass fractionation assuming ^{186}W/^{184}W = 0.92767. The measured ^{182}W/^{184}W and ^{183}W/^{184}W ratios are expressed as $\varepsilon_{^xW}\left[\left(^xW/^{184}W\right)_{spl}/\left(^xW/^{184}W\right)_{std}-1\right]\times 10{,}000$ with $x = 182$ or 183 using an Alfa Aesar

Table 2
Blank-corrected Pb isotope compositions and Pb and U concentrations for troilite inclusions in the Muonionalusta and Gibeon iron meteorites.

Sample	$^{206}Pb/^{204}Pb$	$^{204}Pb/^{206}Pb$	2s%	$^{207}Pb/^{206}Pb$	2s%	$^{208}Pb/^{206}Pb$	2s%	ng Pb	ng U	μ	T_{CD} (Ga)	±2s
Muonionanlusta Slab 1 Run 0 (1.59 g; no Fe extraction)												
ML1-L1-N0.5	22.267	0.044910	46.3	0.82811	15.86	1.66774	46.2	0.721	0.033	12.6		
ML1-L2-N0.5	25.119	0.039810	2.9	0.80257	0.50	1.46313	3.38	2.69	0.142	15.3	4.563	0.004
ML1-L4-HF8	47.223	0.021176	282	0.71400	110.90	0.69000	300	0.182	0.019	36.8		
ML1-R-0-2-CN	63.741	0.015689	67.1	0.69539	4.94	0.47343	102	1.07	0.122	52.8	4.568	0.006
Muonionanlusta Slab 1 Run R1 (2.18 g; no Fe extraction)												
ML1-R1-L1-N1	20.917	0.047809	2.4	0.84074	0.26	1.79427	2.68	2.00	0.084	11.3	4.573	0.010
ML1-R1-L2-N1	37.558	0.026626	7.0	0.74216	0.88	1.01980	6.89	3.23	0.243	27.4	4.560	0.003
ML1-R1-L3-N1	45.735	0.021865	184	0.72165	55.11	0.76636	199	0.354	0.034	35.3		
ML1-R1-L4-HF50	32.216	0.031040	180	0.77692	59.17	1.04795	196	0.263	0.019	22.2		
ML1-R1-R-CN	71.785	0.013931	134	0.68728	15.88	0.42367	150	0.826	0.100	60.6	4.568	0.016
Muonionanlusta Slab 1 Run R2 (2.45 g; no Fe extraction)												
ML1-R2-L1-N1	134.78	0.007420	17.1	0.65491	0.62	0.35188	11.8	5.25	0.691	122	4.559	0.001
ML1-R2-L2-N1	1017.2	0.000983	61.0	0.62817	0.24	0.11599	23.0	18.55	3.113	978	4.564	0.000
ML1-R2-L2-N1-rr	1072.3	0.000933	122	0.62800	0.37	0.11439	24.3	10.15	1.805	1031	4.564	0.000
ML1-R2-L3-N1	248.07	0.004031	29.7	0.64088	0.51	0.22681	21.0	9.10	1.337	232	4.562	0.001
ML1-R2-L4-HF50	121.95	0.008200	218	0.65922	35.15	0.37371	192	0.585	0.089	109	4.562	0.013
ML1-R2-R-CN	196.22	0.005096	357	0.64505	82.13	0.21395	350	0.280	0.070	181	4.564	0.117
Muonionanlusta Slab 2 Run sa1 (2.80 g; Fe extraction)												
ML2-sa1-L1-N1	20.051	0.049873	0.5	0.84233	0.08	1.90710	0.48	4.55	0.178	10.4	4.539	0.003
ML2-sa1-L2-N1	22.352	0.044739	68.4	0.82116	25.15	1.68814	68	0.494	0.023	12.7		
ML2-sa1-L3-HF50	18.712	0.053441	70.3	0.85999	33.24	2.07966	7.15	0.130	0.005	9.1		
ML2-sa1-L4-N1	20.103	0.049745	82.6	0.83836	44.51	1.88518	84	0.291	0.012	10.5		
Muonionanlusta Slab 2 Run sa2 (2.65 g; no Fe extraction)												
ML2-sa2-L1-N1	17.991	0.055584	0.1	0.86952	0.06	2.10224	0.03	7.35	0.244	8.4	4.543	0.002
ML2-sa2-L2-N1	18.676	0.053544	30.4	0.85436	1.65	2.01599	36	0.326	0.012	9.1		
ML2-sa2-L3-HF50	17.420	0.057405	2.3	0.89196	1.61	2.13821	0.98	1.23	0.039	7.9	4.617	0.054
ML2-sa2-L4-N1	20.459	0.048878	115	0.84250	39.34	1.89028	102	0.105	0.004	10.8		
Muonionanlusta Slab 1 Run R5 (3.10 g; Fe extraction)												
ML1-R5-L1-N1	19.674	0.050829	0.4	0.84628	0.05	1.94373	0.38	4.90	0.186	10.1	4.536	0.002
ML1-R5-L2-N1	21.237	0.047088	5.0	0.83010	0.93	1.80109	5.28	1.42	0.060	11.6	4.542	0.015
ML1-R5-L3-N1	22.446	0.044551	4.2	0.81773	0.90	1.69864	4.37	1.60	0.073	12.7	4.539	0.010
ML1-R5-L4-N1	30.515	0.032770	20.4	0.76737	2.61	1.25572	20.2	1.25	0.080	20.6	4.552	0.007
ML1-R5-L5-N1	28.275	0.035367	115	0.77731	35.06	1.35425	115	0.427	0.026	18.4		
ML1-R5-L6-N1	18.974	0.052703	0.2	0.83964	0.07	2.03397	0.10	5.60	0.201	9.4	4.463	0.002
ML1-R5-L7-HF50	27.339	0.036578	112	0.78380	35.50	1.40489	108	0.434	0.025	17.5		
ML1-R5-L8-N1	26.340	0.037964	81.4	0.79235	25.22	1.43180	72.6	0.574	0.032	16.5	4.560	0.125
ML1-R5-L9-CHCl	45.263	0.022093	310	0.72512	145.57	0.88262	307	0.137	0.014	34.9		
ML1-R5-R-CN	18.517	0.054006	14.7	0.85563	1.01	2.05987	6.79	1.08	0.038	8.9	4.511	0.051
Muonionanlusta Slab 1 Run H (3.01 g; Fe extraction)												
ML1-H-L1-N1	19.002	0.052626	0.2	0.85382	0.004	2.00788	0.13	7.00	0.253	9.4	4.533	0.002
ML1-H-L2-N1	19.670	0.050838	0.4	0.85829	0.02	1.90680	0.44	5.25	0.201	10.1	4.590	0.004
ML1-H-L3-N1	25.586	0.039084	5.2	0.79435	0.86	1.49216	5.21	2.47	0.131	15.8	4.545	0.004
ML1-H-R-CN	67.413	0.014834	48.6	0.68861	3.58	0.58865	43.7	1.95	0.209	56.4	4.560	0.003
Muonionanlusta Slab 2 Run I (3.49 g; Fe extraction)												
ML2-I-L1-N1	18.908	0.052888	0.1	0.85613	0.002	2.00363	0.06	12.6	0.453	9.3	4.538	0.001
ML2-I-L2-N1	19.921	0.050198	0.4	0.84426	0.08	1.87009	0.69	5.25	0.206	10.3	4.540	0.002
ML2-I-L3-N1	22.270	0.044904	5.7	0.82061	0.97	1.61840	9.60	1.70	0.079	12.6	4.544	0.007
ML2-I-R-CN	26.674	0.037490	7.3	0.79028	1.17	1.28486	13.7	3.07	0.178	16.8	4.557	0.010
Muonionanlusta Slab 1 Run J (3.38 g; Fe extraction)												
ML1-J-L1-N1	18.424	0.054278	0.2	0.85689	0.06	2.08760	0.02	4.90	0.168	8.8	4.511	0.003
ML1-J-L2-N1	18.983	0.052678	0.1	0.84211	0.02	2.04933	0.02	17.85	0.639	9.4	4.476	0.000
ML1-J-L3-N1	22.154	0.045138	16.0	0.80957	14.40	1.75759	15.4	3.44	0.153	12.5	4.493	0.005
ML1-J-R-CN	27.837	0.035924	5.2	0.77570	0.94	1.38702	5.00	2.49	0.144	18.0	4.530	0.003
ML1-J-R-CN-rr	27.478	0.036393	0.9	0.77764	0.18	1.40242	0.87	9.80	0.559	17.6	4.529	0.001
Gibeon (3.32 g; Fe extraction except for leach fractions L2 and L6)												
Gib-L1-N1	20.060	0.049850	0.1	0.83169	0.03	1.88984	0.10	21.7	0.855	10.4	4.491	0.000
Gib-L2-N1	20.330	0.049188	0.7	0.82812	0.20	1.86224	0.76	5.60	0.225	10.7	4.489	0.001
Gib-L3-N2.5	33.787	0.029597	7.0	0.75585	0.86	1.08139	7.80	3.50	0.246	23.7	4.561	0.003
Gib-L4-N7	28.294	0.035343	3.1	0.78326	0.50	1.31189	3.34	3.50	0.209	18.4	4.566	0.003
Gib-L5-N7	61.720	0.016202	40.4	0.70647	3.94	0.52988	68.1	1.45	0.157	50.8	4.592	0.005
Gib-L6-N7	71.829	0.013922	311	0.69036	103.11	0.42731	337	0.193	0.028	60.7		

R = Residue; L = Leachate; N0.5, N1, N2.5, and N7 = 0.5 N, 1 N, 2.5 N, and 7 N HNO_3, respectively; CN = Concentrated HNO_3; HF8 and HF50 = 8 N and 50% HF, respectively; CHCl = Concentrated HCl; rr = rerun; 2s = 2 sigma; $\mu = {}^{238}U/{}^{204}Pb$.
When a leachate or residue fraction is missing for a sample it is because it did not contain enough Pb to carry out a statistically significant isotope analysis.

Table 3
NIST 981 standard values.

Sample	$^{206}Pb/^{204}Pb$	±2s	$^{207}Pb/^{204}Pb$	±2s	$^{208}Pb/^{204}Pb$	±2s	$^{207}Pb/^{206}Pb$	±2s	$^{208}Pb/^{206}Pb$	±2s
NIST 981 standard										
This work[a]	16.9370	0.0067	15.4921	0.0053	36.700	0.011	0.91469	0.00015	2.16687	0.00057
Eisele et al. (2003)	16.9409	0.0019	15.4976	0.0024	36.7262	0.0086	0.91480		2.16790	

[a] Tl-normalized, before S/S bracketing.

W standard (stock #35770, lot #233665H), which was analyzed before, in between, and after each sample, which was run twice, to allow for sample-standard bracketing.

3. Least-square methods

ISOPLOT, the most widely used isochron software (Ludwig, 2003), treats coordinates as normal (Gaussian) variables. It is well known that the normal approximation may turn out to be poor for isotopic ratios. This can be easily understood by considering the two isotopic ratios, $^{204}Pb/^{206}Pb$ and $^{207}Pb/^{206}Pb$, and assuming that they are both normal variables. The ratio of two normal variables is known to be, not a normal, but a Cauchy variable with the unpleasant property that it does not have finite variance and standard-deviation (e.g., Hoel et al., 1971). In the present case, this is equivalent to the ratio $^{207}Pb/^{204}Pb$ of the two variables not being a normal variable itself. Yet, although isotope ratios cannot be negative values, the assumption of a normal variable is usually harmless. Occasionally, however, and in particular for very radiogenic samples such as those handled here, this assumption breaks down. Conspicuous cases of measurements involving error ellipses that encroach into the half-space of negative ratios are the angrites analyzed by Amelin (2008) and the Allende CAIs analyzed by Jacobsen et al. (2008): assuming a non-zero probability that an isotopic ratio is negative carries no physical meaning.

We therefore wrote a new code for a least-square straight-line that assumes that the isotopic ratios are log-normal variables, a property that carries over to ratios of ratios. We actually use a first-order approximation of correlated normal errors. Error surfaces appear as warped ellipses (see below), but would show up as regular ellipses in a log–log plot. The equations behind this code are described in Appendix A. Errors on the slope and the intercept are propagated by Monte-Carlo loops (e.g., Albarède, 1995), usually as many as 2000. The ranges of ages given are obtained by removing 2.5% of both the oldest and the youngest ages.

4. Results

The blank-corrected Pb isotope data for Muonionalusta and Gibeon troilite, together with the sample weights and whether or not Fe extraction was performed, are listed in Table 2 in their chronological run order and shown in Figs. 1–3. The W isotope data for Muonionalusta iron are listed in Table 4. The errors in percent in Table 2 are relative as expected from a lognormal distribution (if x is a lognormal variable then $y = \ln x$ is normal). A relative error of ϵ indicates that the limits of the confidence interval are obtained by multiplying and dividing the mean by e^{ϵ}, or by $(1+\epsilon)$ if $\epsilon \ll 1$. Large errors on $^{204}Pb/^{206}Pb$ ratios reflect large, conservative blank corrections, while $^{207}Pb/^{206}Pb$ is much less affected, hence preserving a good precision on the ages.

The Pb isotope compositions of most of the leachates and residues of Muonionalusta are more radiogenic than common terrestrial Pb. The range of $^{206}Pb/^{204}Pb$ is quite variable from one troilite sample to another. Common to all sample splits, however, is that they contained only very little Pb (0.1 to 19 ng), at least two orders of magnitude less than, for example, Canyon Diablo or Nantan, both of which, for the same amount of troilite processed (data to be published elsewhere), contain large quantities of Pb (i.e., their troilite Pb concentrations are much higher than those of Muonionalusta and Gibeon troilite). Slab ML1, in particular, was found to contain troilite with highly radiogenic Pb, with $^{206}Pb/^{204}Pb$ ranging up to 1072, that forms an array in the reverse $^{207}Pb/^{206}Pb$ and $^{208}Pb/^{206}Pb$ vs $^{204}Pb/^{206}Pb$ isochron plots (Fig. 1). These isotopic ratios correspond to apparent μ ($^{238}U/^{204}Pb$) values of up to 1000, which is unexpected for a sulfide. Slab ML2 contained Pb that was only moderately radiogenic compared to the Pb from ML1, and although this Pb falls on the same array as defined by ML1, the ML2 Pb isotopic compositions do not define useful alignments (Fig. 2). In contrast to the uranogenic Pb, $^{208}Pb/^{206}Pb$ values are very low for both slabs, attesting to low Th/U ratios in the Muonionalusta troilite material as a whole. Subsamples ML1-run 0 and ML1-R1 plot below the other subsamples. Lead from the six fractions of Gibeon also is more radiogenic than common terrestrial Pb but, as for ML2, not nearly as radiogenic as Pb from ML1, and plots on the array delineated by ML1 and ML2 together (Fig. 3). Like Muonionalusta, Gibeon contained only very little Pb (36 ng total Pb for the 3.5 g troilite chunk analyzed here, i.e., ~10 ppb, consistent with the LA-ICP-MS estimate).

We furthermore computed the $^{207}Pb^*/^{206}Pb^*$ ages obtained by removing primordial Pb (Table 2). For consistency and improved precision over literature values, we used for primordial Pb the isotopic composition of the least radiogenic Pb we could identify and measure during the course of this study, which was Pb from troilite nodules in the IAB-IIICD iron meteorite Nantan ($^{204}Pb/^{206}Pb = 0.10743(4)$, $^{207}Pb/^{206}Pb = 1.1047(3)$, and $^{208}Pb/^{206}Pb = 3.1596(9)$; complete data set to be published elsewhere). Nantan is particularly rich in Pb (tens of ppm), more so even than Canyon Diablo, and its Pb isotope composition has already been found to be indistinguishable within error from that of Canyon Diablo (Chen and Wasserburg, 1983). We nevertheless kept the symbol T_{CD} to represent the apparent $^{207}Pb^*/^{206}Pb^*$ ages (Table 2).

The overall alignment of all the Muonionanlusta data from slab ML1 is consistent with an unrealistically old age of 4573 ± 3 Ma (Fig. 1a), but, as attested to by the very large MSWD of 17, it is affected by visible scatter due to variable proportions of terrestrial and primordial Pb. A $^{232}Th/^{238}U$ of ~0.3 is estimated, assuming a $^{208}Pb^*/^{206}Pb^*$ value of ~0.08 (Fig. 1b) and the relationship:

$$\frac{^{208}Pb^*}{^{206}Pb^*} = \frac{^{232}Th}{^{238}U} \times \frac{e^{\lambda_{^{232}Th}T} - 1}{e^{\lambda_{^{238}U}T} - 1}$$

where T is the age. HF leachates are systematically anomalous, which may reflect the presence of tiny silicate minerals for which terrestrial contamination cannot be excluded. The data on slab ML2 define a very poor alignment with an apparent age of 4556 ± 3 Ma in $^{207}Pb/^{206}Pb$–$^{204}Pb/^{206}Pb$ space (Fig. 2a), again with a high MSWD of 11. Likewise, the alignment in the $^{208}Pb/^{206}Pb$ vs $^{204}Pb/^{206}Pb$ plot is rather mediocre (Fig. 2b), yet the initial $^{208}Pb/^{206}Pb$ is clearly very low. The six fractions of Gibeon also define an unrealistically old Pb–Pb age of 4634 ± 2 Ma (Fig. 3a) with an MSWD of 45. The apparent initial $^{208}Pb/^{206}Pb$ of −0.12 (Fig. 3b) is inconsistent with a simple binary mixture of primordial and radiogenic Pb. Again, the conspicuous presence of U-rich domains is attested to by the highest μ value of 60 (Table 2).

As already mentioned in the methodology section, the isotopic composition of U could not be measured for lack of large enough ion beam signals. This may be due to the presence of small amounts of sulfate in the chemistry (derived from the oxidation of sulfur during

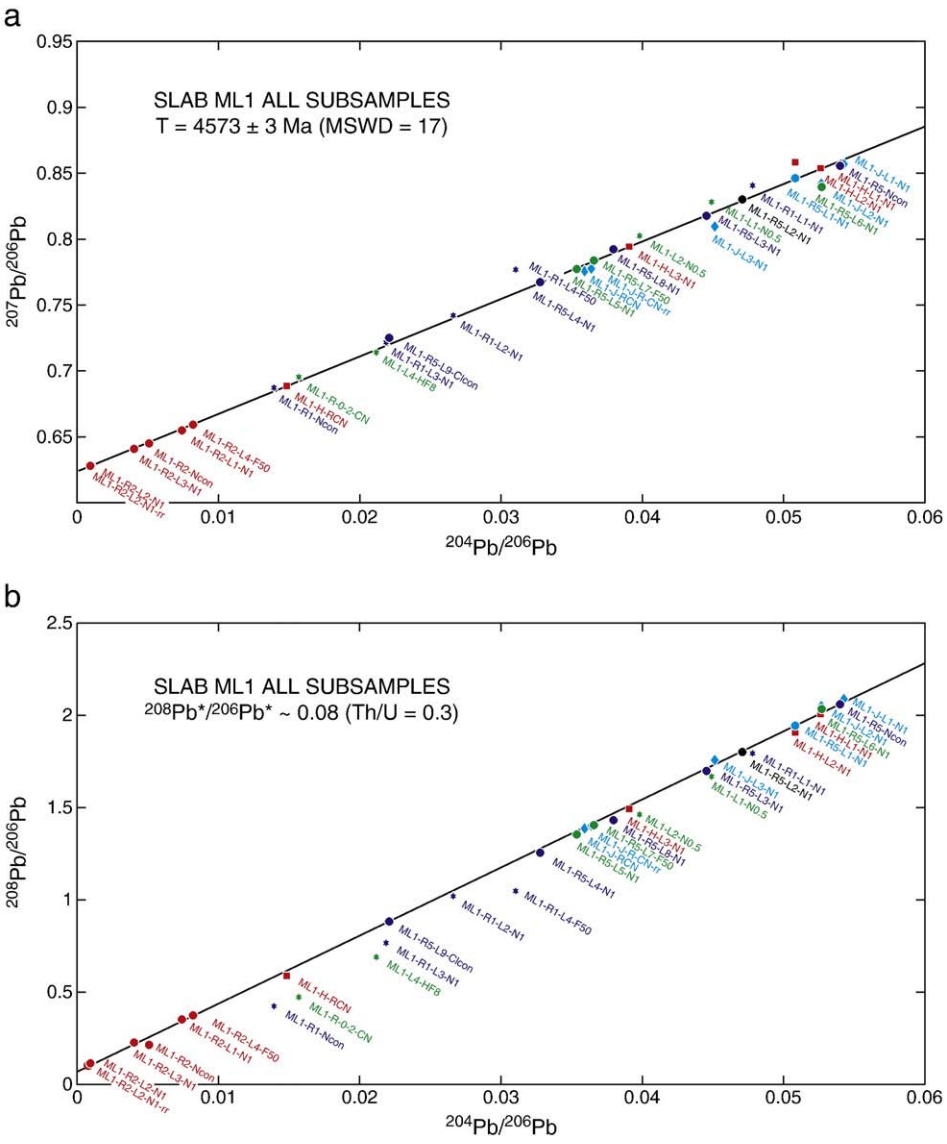

Fig. 1. Plot of $^{207}Pb/^{206}Pb$ (a) and $^{208}Pb/^{206}Pb$ (b) vs $^{204}Pb/^{206}Pb$ for different subsamples from slab 1 of Muonionalusta. Refer to Table 2 for error bars, which are, in general, smaller than the symbol size and, hence, for legibility, error ellipses have been omitted. All the data are blank corrected. The different colors refer to different subsamples also distinguished by their run numbers (0, R1, R2, R5, H, and J; see Table 2). L = leachate; R = residue; L1, L2, … etc. = first leach, second leach, etc.; N = HNO_3; Cl = HCl; H, F, HF = HF; N0.5, N1 = 0.5 N, 1 N HNO_3; Ncon = concentrated HNO_3; RCN = residue concentrated HNO_3; HF8 = 8 N HF; F50 = HF 50%; rr = rerun. In (a) the intercept $^{207}Pb^*/^{206}Pb^*$ is a measure of the age. The age recorded by the entire sample set in (a) is not significant as indicated by the large MSWD. Different subsamples show different degrees of contamination, but $^{204}Pb/^{206}Pb$ occasionally reflects very high U/Pb ratios. In (b) the intercept $^{208}Pb^*/^{206}Pb^*$ (~0.08) is a measure of the $^{232}Th/^{238}U$ ratio (≈Th/U) (~0.3) prevailing during the evolution of the sample.

sample dissolution) replacing U on the resin, or to insoluble U-rich phases, which would require dissolution in high-pressure bombs, the use of which we have deliberately been avoiding in order to keep Pb blanks as low as possible.

The W isotope results obtained on the Muonionalusta iron next to the troilite inclusions from both ML1 and ML2 are consistent with literature data (Horan et al., 1998; Scherstén et al., 2006; Markowski et al., 2006; Qin et al., 2008) with ε_0 values of −3.0 and −3.4 (in parts per 1/10,000). The ^{182}Hf–^{182}W ages with respect to CAIs (Kleine et al., 2005) correspond to 2.4 ± 2.0 Ma. The results for Muonionalusta also compare well with the data of Qin et al. (2008) on Gibeon with $\varepsilon_0 = -3.38 \pm 0.05$.

5. Discussion

5.1. Pb–Pb chronology and the evolution of the IVA parent body

The data were processed in the reverse $^{207}Pb/^{206}Pb$ and $^{208}Pb/^{206}Pb$ vs $^{204}Pb/^{206}Pb$ isochron plots, which minimize correlations between variables. When all the Pb fractions of slab ML1 are considered, an unrealistically old age of 4573 ± 3 Ma is obtained (Fig. 1a) but, as attested to by the high MSWD (~17), the scatter is very large. This is due in part to the error bars on our samples, which are smaller by one to two orders of magnitude compared to those for literature data (e.g., Amelin, 2008; Jacobsen et al., 2008) as a result of the larger amounts of Pb necessary for analysis by MC-ICP-MS compared to TIMS. However, a preliminary decomposition of the data set by Principal Component Analysis demonstrates that the three principal components account for, respectively, 99.65, 0.31, and 0.03% of the variance: this is a clear indication that a binary mixture between radiogenic and unradiogenic Pb does not fully account for the observations. We therefore tested the hypothesis that three types of Pb are present in the samples, radiogenic Pb, primordial Pb (Canyon Diablo-like, hereafter CD), and terrestrial Pb (e.g., Stacey and Kramers, 1975, hereafter SK). The latter component, which in some fractions is surprisingly abundant, can conveniently be lumped together with Pb from the blank. The data were regressed in the $^{207}Pb/^{206}Pb$, $^{208}Pb/$

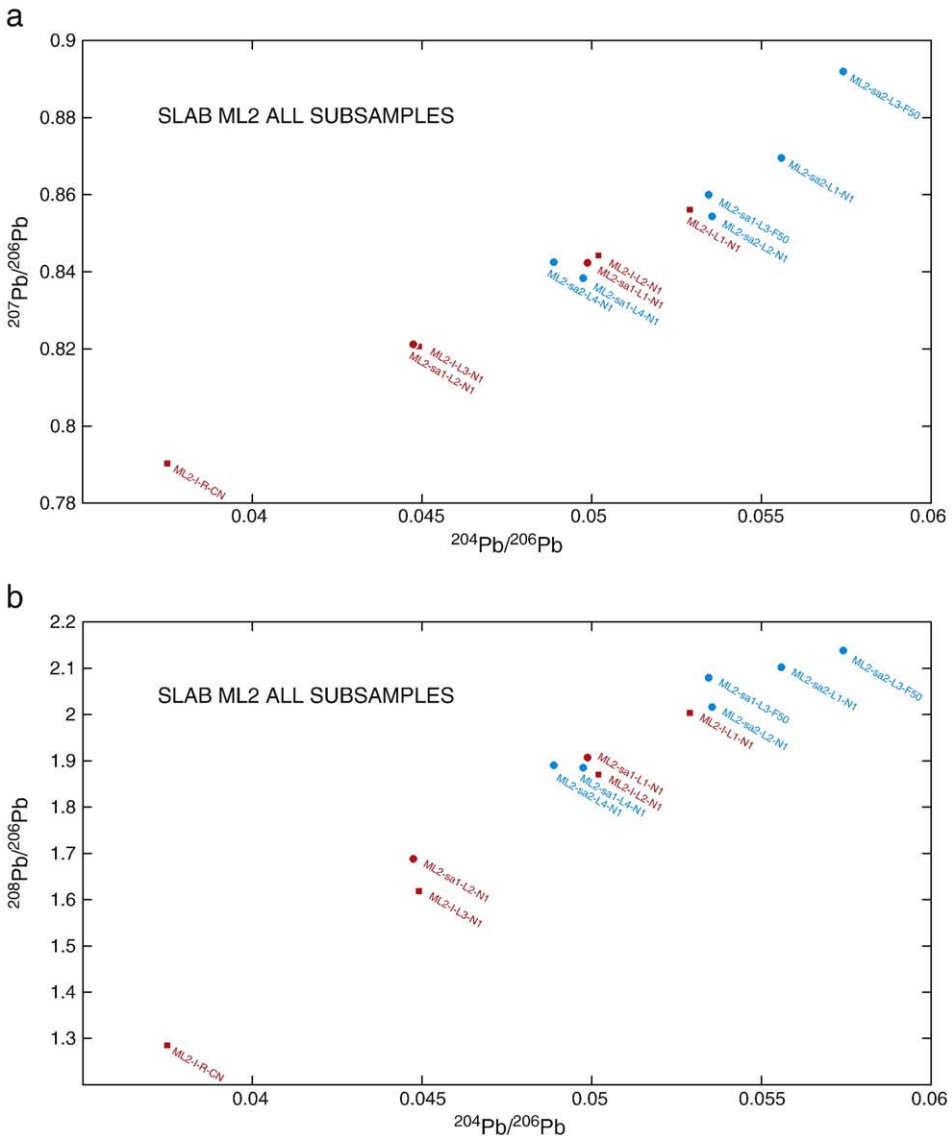

Fig. 2. Plot of $^{207}Pb/^{206}Pb$ (a) and $^{208}Pb/^{206}Pb$ (b) vs $^{204}Pb/^{206}Pb$ for different subsamples from slab 2 of Muonionalusta. See caption of Fig. 1 and Table 2 for symbol key and run numbers (sa1, sa2, and I). All the samples are much less radiogenic than those from slab 1. No significant age is defined in (a) and no significant Th/U ratio can be derived from (b).

^{206}Pb, and $^{204}Pb/^{206}Pb$ tri-dimensional space. The assumption that the plane goes through both CD and SK can be graphically seen to hold by comparing the observed $^{208}Pb/^{206}Pb$ of the samples with their estimated values (Fig. 4).

One conclusion, therefore, is that, because of the presence of two non-radiogenic Pb components, only the most radiogenic fractions should be used to obtain an age. The subsample ML1-R2 has surprisingly high $^{206}Pb/^{204}Pb$ of over 1000 and, hence, suggests that ML1 is the most promising sample for chronology. A precise age of 4565.3 ± 0.1 Ma (MSWD = 0.08) is obtained for this sample (Fig. 5a), which is the most ancient Pb–Pb age obtained so far for a differentiated planetary object, older even than the age of the angrite d'Orbigny, which was dated by Amelin (2008) at 4564.4 ± 0.1 Ma. This age is close, but not identical to the oldest values of $T_{CD} = 4564.4$ Ma of the samples with the lowest $^{204}Pb/^{206}Pb$ ratios (Table 2).

It has been suggested recently that the $^{238}U/^{235}U$ ratio may vary in CAIs as a consequence of the presence of ^{247}Cm ($T_{1/2} = 15.6$ Ma) at the time of their formation and, hence, increase their apparent Pb–Pb ages by up to a few Ma (Brennecka et al., 2010a). It has also been established, however, that U in bulk carbonaceous and ordinary chondrites lacks significant isotopic anomalies (Stirling et al., 2005, 2006), which seem to be restricted to low-temperature environments with redox contrasts (Weyer et al., 2008; Brennecka et al., 2010b). We therefore consider that the ages reported in the present work are unlikely to be affected by the in-situ decay of ^{247}Cm.

The cooling rate of IVA irons decreases from >3000 to 200 K Ma^{-1} when Ni contents increase from 7 to 13 wt.% (Rasmussen et al., 1995; Yang et al., 2007, 2008). The positive correlation of Ni and Au in IVA irons indicates that Ni preferentially remains in the liquid (i.e., is incompatible) during iron solidification (Wasson and Richardson, 2001). Cooling rates therefore decrease while solidification proceeds as latent heat becomes progressively more difficult to extract. Crystallization of the IVA irons seems to be taking place inward (Yang et al., 2007), presumably by dendritic growth (Haack and Scott, 1992). Contrary to planets in which the inner core grows, modelling such an asteroidal core is not well understood (Nimmo, 2009).

The present Pb–Pb age of 4565.3 ± 0.1 Ma for ML1 is consistent with the ^{182}Hf–^{182}W metal–silicate segregation age of 2.4 ± 2.0 Ma for ML1 and ML2 with respect to the CAI isochron of Kleine et al. (2005), regardless of which estimate (4567.1–4568.7 Ma) of the CAI Pb–Pb age is considered (Bouvier et al., 2007; Amelin and Krot, 2007;

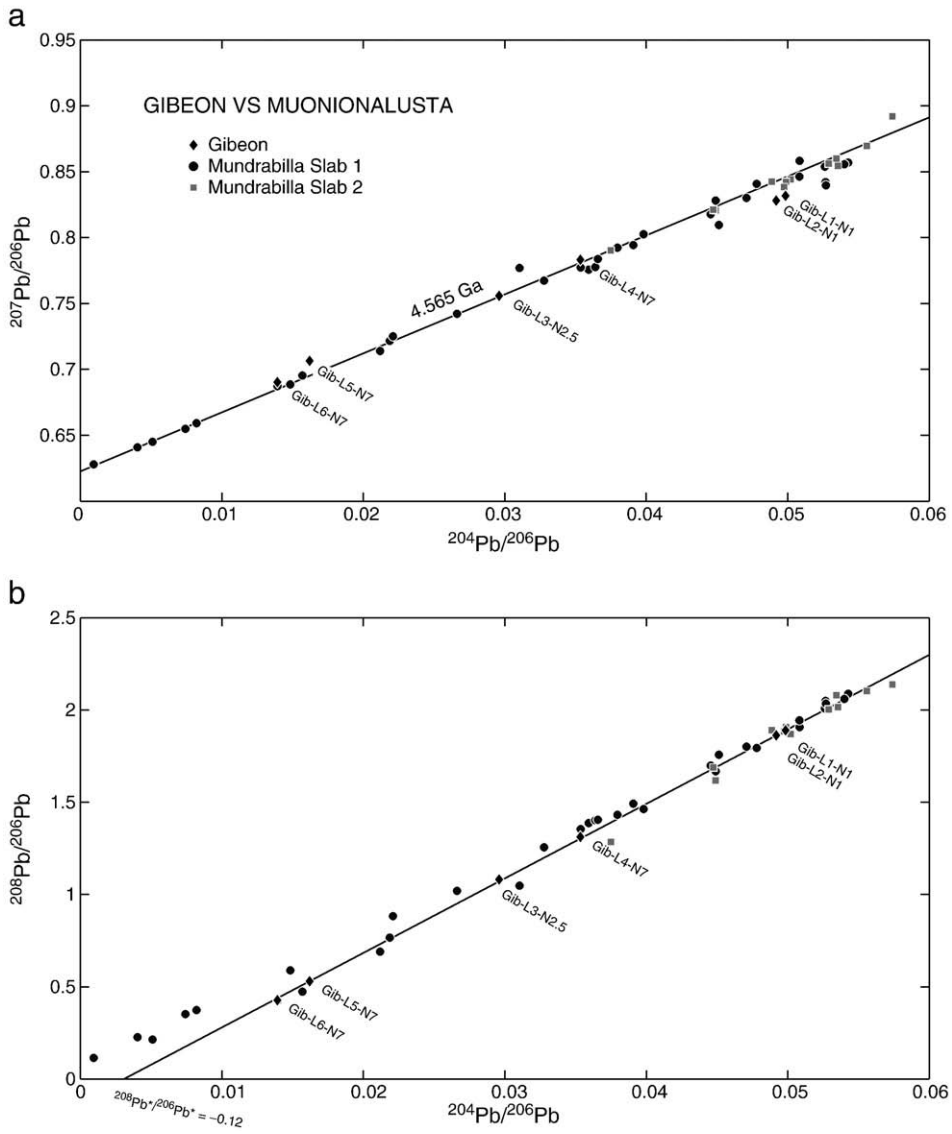

Fig. 3. Comparison of the Gibeon (diamonds) and Muonionalusta data (circles and squares) in plots of $^{207}Pb/^{206}Pb$ (a) and $^{208}Pb/^{206}Pb$ (b) vs $^{204}Pb/^{206}Pb$. L1–L6 = leachates 1–6; N1, N2.5, N7 = 1 N, 2.5 N,7 N HNO_3. (a) The 4.565 Ga isochron is shown for reference only. Leachates L1 and L2 are most likely mixtures of common terrestrial and primordial Pb with radiogenic Pb. (b) In spite of a good alignment of the six Gibeon fractions that spread over a large interval of $^{204}Pb/^{206}Pb$ values in (a), the negative intercept $^{208}Pb^*/^{206}Pb^*$ of −0.12 suggests that the U–Th–Pb system was disturbed after troilite formation.

Connelly et al., 2008; Jacobsen et al., 2008; Wadhwa and Bouvier, 2009). Using a Ni content of 8.4 wt.% for Muonionalusta iron (Rasmussen et al., 1995), a cooling rate of about 500 K Ma^{-1} can be deduced from the calculations of Yang et al. (2007, 2008), which leaves 2–3 Ma after CAIs for the metal to reach 300 °C, the closure temperature for Pb in sulfide, which we take to be similar to that of Os (Brenan et al., 2000). This implies that the IVA parent body accreted within 1 Ma of CAI formation. Given the different events recorded by the Pb–Pb and Hf–W chronometers, there should be no a priori expectation of obtaining identical ages when comparing these two systems to each other. However, when overlap of Pb–Pb and Hf–W high-precision ages is observed, such as in the present study, that would require very rapid progression from segregation to cooling, and therefore the likelihood of a small, or rapidly fragmented, body.

Table 4
W isotope compositions for Muonionalusta iron.

Sample	$\varepsilon_{^{182}W}$	±2s	$\varepsilon_{^{183}W}$	±2s
Muonionalusta slab 1	−3.33	0.19	0.04	0.18
	−3.04	0.39	0.36	0.29
Muonionalusta slab 2	−3.03	0.20	0.09	0.16
	−3.42	0.34	−0.35	0.27

The unrealistically old Pb–Pb age and associated scatter of Gibeon clearly are due to the first two leachates, which extracted Pb with terrestrial characteristics (blank or contamination). The other four fractions define a rather young age of 4544 ± 7 Ma with an MSWD = 1.5 (Fig. 6), suggesting that the alignment may be statistically significant. They also form a good alignment in the $^{208}Pb/^{206}Pb$ vs $^{204}Pb/^{206}Pb$ plot (Fig. 3b), but the negative intercept (−0.14) indicates that the $^{204}Pb/^{206}Pb$ of the most radiogenic samples is too low and that the Pb–Pb age is too young. This age is, however, almost within error of the ^{107}Pd–^{107}Ag age of 8.5 + 3.2/−4.6 Ma (Schönbächler et al., 2008) with respect to chondrites. Taken together, available chronological evidence therefore confirms petrological observations (Buchwald, 1975; Teshima et al., 1986) that all the troilite nodules from Gibeon were shock-melted. We thus propose

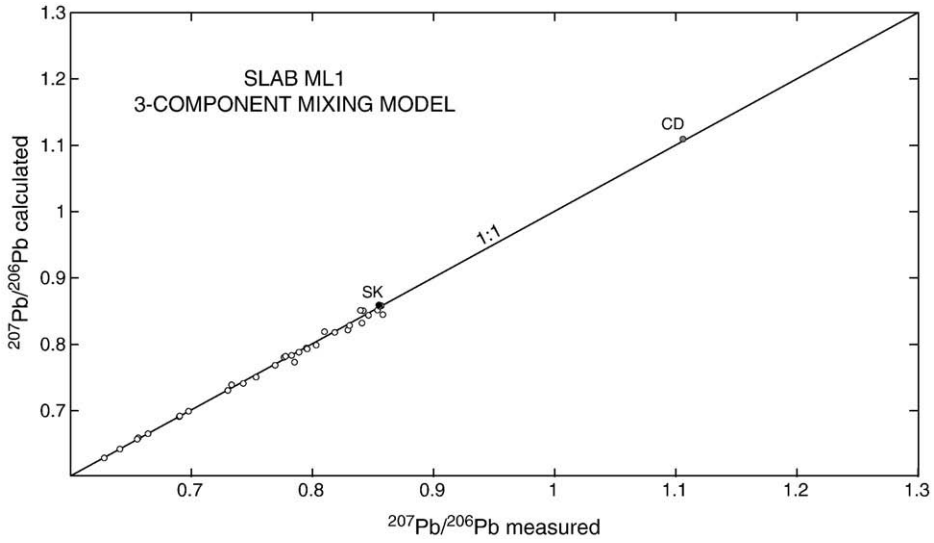

Fig. 4. Fit of the 3-component end-member mixing model for slab 1 of Muonionalusta. It is assumed that Pb in the samples represent mixtures of common terrestrial and primordial components with radiogenic Pb. SK stands for common terrestrial Pb and is assigned the values determined by Stacey and Kramers (1975), while CD has been given our unpublished values of Nantan, which is very close to the literature values for Canyon Diablo. The variable $z = {}^{207}Pb/^{206}Pb$ is linearly regressed against $x = {}^{204}Pb/^{206}Pb$ and $y = {}^{208}Pb/^{206}Pb$ and the plot shows the adjusted (calculated) value of z vs its measured value. The good fit suggests that a large part of the scatter, such as seen in Figs. 1–3 is due to the non-binary character of the Pb isotope composition and that emphasis should be on the most radiogenic data, especially on the ML1-R2 subsample.

that the apparent Pb–Pb, and possibly Pd–Ag, ages of Gibeon were reset by volatilization upon shock melting. This is our best hypothesis for why troilite inclusions in two IVA iron meteorites, which, as testified to by their similar Ni contents, evolved to a similar extent and presumably formed at roughly the same time, have different Pb–Pb ages.

As inferred here from combined Hf–W and Pb–Pb isotopic evidence, the parent body of Muonionalusta, and most likely of all of the IVA iron meteorites, seems to have formed within 1 Ma after CAIs and cooled to the Pb closure temperature within 2–3 Ma. As discussed by Yang et al. (2007), the IVA planetary object was molten very early on. Formation within 0.7 Ma of CAI allows for heating by ^{26}Al (Hevey and Sanders, 2006) and core formation, especially if the accreting material is itself already hot. In a young disk cluttered by many proto-planetary objects and for bodies that are not already molten, tidal dissipation on non-circular orbits around large planets is an additional major source of internal energy (Peale et al., 1979; Segatz et al., 1988).

5.2. The nature of troilite inclusions in IVA iron meteorites

Although the metal phase from IVA iron meteorites is clearly a cumulate (Wasson and Richardson, 2001), possibly including some trapped melt, the dynamic significance of troilite inclusions is puzzling. At the surface of the Earth, an inclusion with a density ρ of 4.6 g cm^{-3} and a diameter of 2 cm would rise in liquid Fe–Ni alloy with $\rho = 7.8$ g cm^{-3} and a viscosity of 5 mPa s (Sato et al., 2005) with a Stokes velocity of 3 cm s^{-1}. Even with the gravity of a <100 km asteroid, the distance travelled in a year in molten metal by such an inclusion measures in the tens or hundreds of km. Such a large settling velocity contrasts with evidence from cooling rates, typically 100–1500 K Ma^{-1} deduced from the growth of Widmanstätten lamellae and Ni diffusion profiles in metal (Rasmussen et al., 1995; Haack et al., 1996; Yang et al., 2007, 2008), and would be slow enough to allow different parts of the core of the parent body to freeze within 1–8 Ma, in agreement with Hf–W and Pb–Pb ages. The lack of metal/sulfide segregation and the scatter of sulfide inclusions in metal, as well as metal inclusions in sulfide, rather are suggestive of a quench texture with much faster cooling. Suspension of troilite blebs in turbulent movements would demand that gravity is strong enough to sustain vigorous convection and, therefore, that the parent body is large enough to develop a strong gravity field, even in the core, which is not consistent with the rapid cooling of the latter. In addition, none of these observations can account for the presence of small (~0.5 cm) metal blebs *within* the larger sulfide inclusions, such as observed here for Gibeon.

Even though the high U/Pb ratios and low Pb concentrations of troilite from Muonionalusta and Gibeon are consistent with the overall depletion of volatiles in the IVA iron meteorites, what was unforeseen is the high abundance of U (of the order of 100 ppt to 1 ppb) as deduced from the Pb sample size and the μ values, a figure that may be compared with the ~8 ppb in CIs (Lodders, 2003) and essentially no U (~5–7 ppt) in Canyon Diablo (Chen and Wasserburg, 1983; Göpel et al., 1985). These high U abundances and the sulfide/silicate melt partition coefficient $D_U \sim 0.001$ obtained by Wheeler et al. (2006) make it unlikely that the troilite blebs represent sulfide that was ever in equilibrium with a silicate melt (liquid immiscibility). Another possibility is that they represent S-rich interstitial melts trapped within the cumulates that became extremely fractionated upon progressive cooling. This model is consistent with several lines of evidence.

1. The Th/U ratio of the Sun, the terrestrial planets, and most meteorites is remarkably constant (~3.8) (Tilton, 1973; Tatsumoto et al., 1976; Chen and Wasserburg, 1986; Lodders, 2003). This ratio is known to be difficult to change drastically by magmatic processes with the sole exception of when accessory phases, such as phosphates or oxides, come into play. The Th/U ratio of Muonionalusta troilite is most precisely known for the ML1-R2 subsample (0.32; Fig. 5b). It is a factor of 12 lower than the solar value, which indicates that U and Th, two refractory and incompatible elements, were fractionated in the process that led to the formation of troilite inclusions in IVA iron meteorites, possibly by removal of phosphates after reduction of U to its trivalent state.
2. The presence of a SiO_2 phase in Muonionalusta, now transformed into stishovite (Holtstam et al., 2003), is an additional indication of the large degree of crystallization achieved by their parent melts.
3. Sulfur isotope data for Muonionalusta and most other IVA iron meteorites are missing from the literature, but Gibeon is uniquely

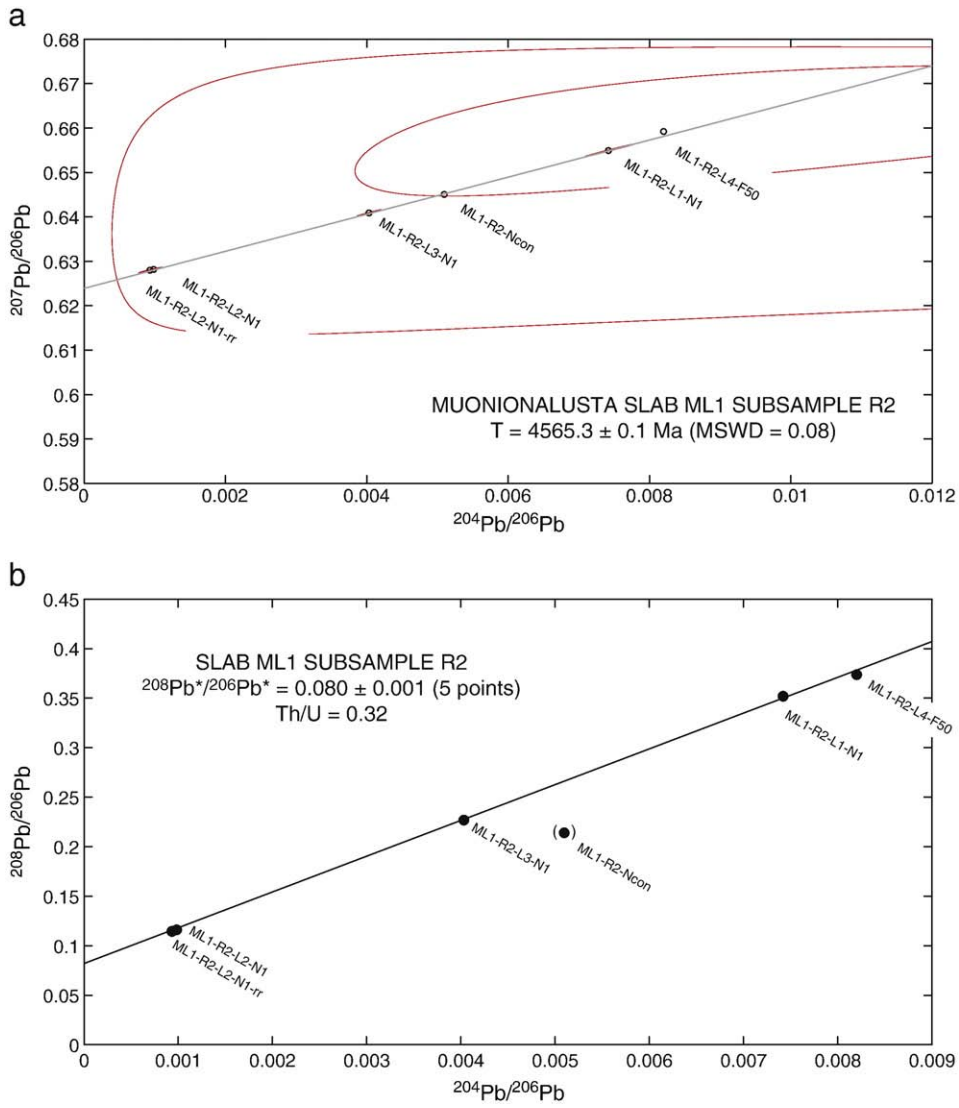

Fig. 5. Pb isotope data for the most radiogenic subsample of Muonionalusta slab 1 (ML1-R2). See caption of Fig. 1 and Table 2 for symbol key and run number (R2). (a) Isochron plot of $^{207}Pb/^{206}Pb$ vs $^{204}Pb/^{206}Pb$ with log-normal error surfaces outlined in red. The intercept defines $^{207}Pb^*/^{206}Pb^*$, which in turn gives the age. The very low MSWD value shows that the age obtained on this subsample is highly significant. This age is the oldest identified so far for a differentiated planetary object. (b) Isochron plot of $^{208}Pb/^{206}Pb$ vs $^{204}Pb/^{206}Pb$: the intercept, calculated here by simple (normal) regression, defines the $^{208}Pb^*/^{206}Pb^*$ ratio, which is converted into a $^{232}Th/^{238}U$ ratio of 0.32.

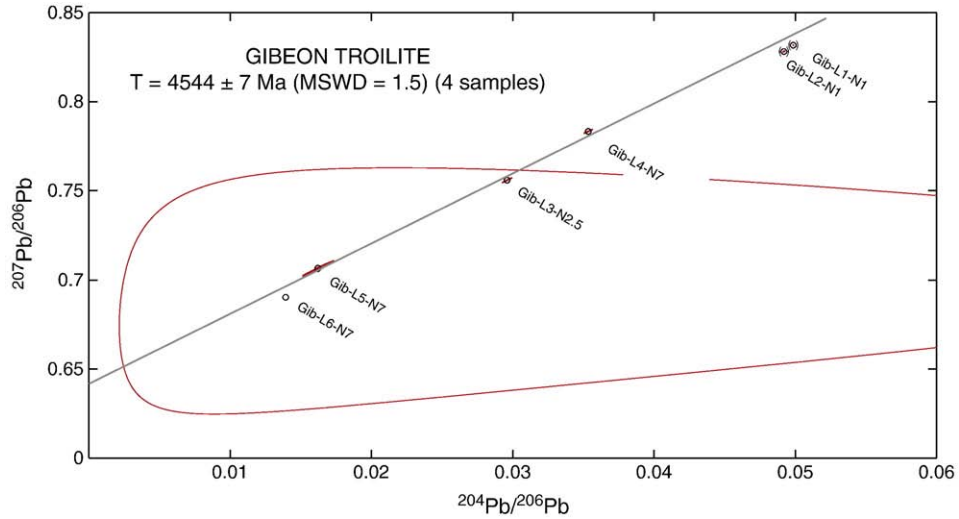

Fig. 6. Isochron plot of $^{207}Pb/^{206}Pb$ vs $^{204}Pb/^{206}Pb$ for the Gibeon troilite sample with log-normal error surfaces outlined in red. See caption of Fig. 3 for symbol key. In spite of a statistically significant alignment, Fig. 3b suggests that the age of 4544 ± 7 Ma may represent that of a perturbation event.

depleted in heavy sulfur isotopes with $\delta^{34}S_{CDT} = -1.20‰$ (Gao and Thiemens, 1991). These authors concluded that such negative values cannot be explained by loss of volatiles during impacts and therefore appeal to a sulfur reservoir with very low $\delta^{34}S$ values and distinct from that of the other meteorites. Sulfur isotope fractionation during the separation of a solid phase with different S packing, such as daubreelite, or liquid–liquid separation, provides an interesting alternative to the existence of a dual S reservoir in the Solar System.

6. Conclusions

Troilite in the Muonionalusta IVA iron meteorite gives a $^{207}Pb^*/^{206}Pb^*$ age of 4565.3 ± 0.1 Ma, consistent with the ^{182}Hf–^{182}W metal–silicate segregation age of 2.4 ± 2.0 Ma. Using literature values for the cooling rate and assuming a closure temperature for Pb of 300 °C suggest that the IVA parent body accreted within 1 Ma of CAI formation. The isotopic composition of Pb in Gibeon troilite gives a significantly younger age of 4544 ± 7 Ma (MSWD = 1.5) in accordance with ^{107}Pd–^{107}Ag evidence, which we interpret as a reset age. High $^{238}U/^{204}Pb$ values of >1000 indicate U concentrations in troilite in the ppt to one ppb range, which may indicate that troilite does not represent metal-sulfide unmixing, but rather corresponds to residual liquids from metal crystallization. The very low $^{232}Th/^{238}U$ of the Muonionalusta troilite (~0.32) requires strong Th/U fractionation, which probably reflect that troilite inclusions formed as late-stage S-rich liquid residues from extreme crystallization of interstitial melts.

Acknowledgements

JBT and FA acknowledge financial support from the French Programme National de Planétologie of the Institut National des Sciences de l'Univers and Centre National d'Etudes Spatiales, and from the French Agence Nationale de la Recherche (grant T-TauriChem), while FM acknowledges financial support from the NASA LASER grant (NNX09AM64G) and CTAL from the Packard Foundation. We thank Luc Labenne and an anonymous meteorite dealer on eBay for providing the samples analyzed in this work. Discussions with Rajdeep Dasgupta were very helpful, as were advice on U column chemistry from Julie Bryce, although U remained at large. We are also very grateful for the constructive and insightful reviews provided by Rich Walker and Mary Horan. We are also indebted to Romain Bouchet and Peter Luffi for help with the LA-ICP-MS analyses. Finally, we thank Alan Levander for providing an inspiring and peaceful work environment during our stay at Rice University as Wiess Visiting Professors.

Appendix A. A least-square straight-line with lognormal errors

We assume that two log-normal distributed x and y variables are measured n times ($i = 1, 2, \ldots, n$). The variables $\alpha = \ln x$ and $\beta = \ln y$ therefore are normally distributed. Using an overbar to signal the estimator of a variable, we test the linear model:

$$\overline{y}_i = a\overline{x}_i + b$$

or, equivalently:

$$e^{\overline{\beta}_i} = ae^{\overline{\alpha}_i} + b. \quad (1)$$

We then form the covariance matrix $\mathbf{S}_i$ of the i-th data:

$$\mathbf{S}_i = \begin{bmatrix} \sigma^2_{x_i} & \sigma_{x_i y_i} \\ \sigma_{x_i y_i} & \sigma^2_{y_i} \end{bmatrix}$$

from the relative variances $\sigma^2_{x_i}$ and $\sigma^2_{y_i}$ and covariance $\sigma_{x_i yi}$. Next, we seek to minimize the sum of squares:

$$s^2 = \sum_{i=1}^{n} \left[\ln\frac{\overline{x}_i}{x_i}, \ln\frac{\overline{y}_i}{y_i}\right] \mathbf{S}_i^{-1} \begin{bmatrix} \ln \overline{x}_i / x_i \\ \ln \overline{y}_i / y_i \end{bmatrix}$$

submitted to n constraints Eq. (1). We therefore introduce n Lagrange multipliers λ_i and seek to minimize the constrained sum of squares γ^2:

$$\gamma^2 = \sum_{i=1}^{n} \left[ln\frac{\overline{x}_i}{x_i}, ln\frac{\overline{y}_i}{y_i}\right] \mathbf{S}_i^{-1} \begin{bmatrix} ln\, \overline{x}_i / x_i \\ ln\, \overline{y}_i / y_i \end{bmatrix} + 2\sum_{i=1}^{n} \lambda_i \left\{ [\overline{x}_i, \overline{y}_i] \begin{bmatrix} a \\ -1 \end{bmatrix} + b \right\}$$

in which the n constraints Eq. (1) appear each with its Lagrange multipliers. We introduce the new variables u_i and v_i such as:

$$\ln \overline{x}_i / x_i = \ln\left(1 + \frac{\overline{x}_i - x_i}{x_i}\right) = \ln(1 + u_i) \approx u_i$$
$$\ln \overline{y}_i / y_i = \ln\left(1 + \frac{\overline{y}_i - y_i}{y_i}\right) = \ln(1 + v_i) \approx v_i$$

in which we assumed that $u_i \ll 1$, i.e., $\ln(1 + u_i) \approx u_i$ (same for v_i).

$$\gamma^2 \approx \sum_{i=1}^{n} [u_i, v_i] \mathbf{S}_i^{-1} \begin{bmatrix} u_i \\ v_i \end{bmatrix} + 2\sum_{i=1}^{n} \lambda_i [ax_i(1 + u_i) - y_i(1 + v_i) + b]$$

We now differentiate γ^2 with respect to each u_i and v_i to find the minimum:

$$d\gamma^2 \approx \sum_{i=1}^{n} 2[du_i, dv_i] \left(\mathbf{S}_i^{-1} \begin{bmatrix} u_i \\ v_i \end{bmatrix} + \lambda_i \begin{bmatrix} ax_i \\ -y_i \end{bmatrix} \right) = 0$$

or equivalently:

$$\begin{bmatrix} u_i \\ v_i \end{bmatrix} = -\lambda_i S_i \begin{bmatrix} ax_i \\ -y_i \end{bmatrix}.$$

We define the weight w_i of the i-th data point as:

$$w_i = w_i(a, b) = [ax_i - y_i] \mathbf{S}_i \begin{bmatrix} ax_i \\ -y_i \end{bmatrix} = a^2 x_i^2 \sigma_{x_i}^2 - 2ax_i y_i \sigma_{x_i y_i} + y_i^2 \sigma_{y_i}^2$$

which gives $\lambda_i = (w_i)^{-1}(ax_i - y_i + b)$ and

$$\gamma^2 \approx \sum_{i=1}^{n} \frac{(ax_i - y_i + b)^2}{w_i}.$$

We can now differentiate γ^2 with respect to the slope a and intercept b at the minimum

$$0 = \frac{1}{2}\frac{\partial \gamma^2}{\partial b} = \sum_{i=1}^{n} \frac{(ax_i - y_i + b)}{w_i}$$
$$0 = \frac{1}{2}\frac{\partial \gamma^2}{\partial a} = \sum_{i=1}^{n} \frac{\left(ax_i^2 - x_i y_i + bx_i\right)}{w_i}.$$

The solution is obtained by solving the following system of two equations in two unknowns:

$$a\sum_{i=1}^{n} \frac{x_i}{w_i} + b\sum_{i=1}^{n} \frac{1}{w_i} = \sum_{i=1}^{n} \frac{y_i}{w_i}$$
$$a\sum_{i=1}^{n} \frac{x_i^2}{w_i} + b\sum_{i=1}^{n} \frac{x_i}{w_i} = \sum_{i=1}^{n} \frac{x_i y_i}{w_i}$$

with respect to a and b. Iterative solutions should quickly converge: a first accurate w_i estimate may be calculated from the values of a and b

obtained by standard regression. Alternatively, the solution may be found by using a Newton–Raphson technique. Errors are calculated by running repeated Monte Carlo cycles. First, a random number generator is used to produce normal deviates, i.e., with zero mean and unit variance, which are easily turned into log-normal deviates. After a proper change of variables using mean values and standard-deviations, the deviates are used to calculate a new set of 'polluted' data x_i and y_i and the system of equations above is solved with the new values. A large number of Monte Carlo cycles, usually >2000, produces reliable estimates of errors and covariance structure.

References

Albarède, F., 1995. Introduction to Geochemical Modeling. Cambridge University Press.

Albarède, F., Telouk, P., Blichert-Toft, J., Boyet, M., Agranier, A., Nelson, B., 2004. Precise and accurate isotopic measurements using multiple-collector ICP-MS. Geochim. Cosmochim. Acta 68, 2725–2744.

Amelin, Y., 2008. U–Pb ages of angrites. Geochim. Cosmochim. Acta 72, 221–232.

Amelin, Y., Krot, A.N., 2007. Pb isotopic age of the Allende chondrules. Meteoritics Planet. Sci. 42, 1321–1335.

Bouvier, A., Blichert-Toft, J., Moynier, F., Vervoort, J.D., Albarède, F., 2007. Pb–Pb dating constraints on the accretion and cooling history of chondrites. Geochim. Cosmochim. Acta 71, 1583–1604.

Brenan, J.M., Cherniak, D.J., Rose, L.A., 2000. Diffusion of osmium in pyrrhotite and pyrite: implications for closure of the Re–Os isotopic system. Earth Planet. Sci. Lett. 180, 399–413.

Brennecka, G.A., Weyer, S., Wadhwa, M., Janney, P.E., Zipfel, J., Anbar, A.D., 2010a. $^{238}U/^{235}U$ variations in meteorites: extant ^{247}Cm and implications for Pb–Pb dating. Science 327, 449–451.

Brennecka, G.A., Borg, L.E., Hutcheon, I.D., Sharp, M.A., Anbar, A.D., 2010b. Natural variations in uranium isotope ratios of uranium ore concentrates: understanding the $^{238}U/^{235}U$ fractionation mechanism. Earth Planet. Sci. Lett. 291, 228–233.

Buchwald, V.F., 1975. Handbook of Iron Meteorites, Their History, Distribution, Composition, and Structure, Vol. 3. University of California Press, Berkeley.

Campbell, A.J., Humayun, M., Weisberg, M.K., 2002. Siderophile element constraints on the formation of metal in the metal-rich chondrites Bencubbin, Weatherford, and Gujba. Geochim. Cosmochim. Acta 66, 647–660.

Chabot, N.L., 2004. Sulfur contents of the parental metallic cores of magmatic iron meteorites. Geochim. Cosmochim. Acta 68, 3607–3618.

Chen, J.H., Wasserburg, G.J., 1983. The least radiogenic Pb in iron meteorites. Lunar and Planetary Science Conference, Houston.

Chen, J.H., Wasserburg, G.J., 1986. Formation ages and evolution of Shergotty and its parent planet from U–Th–Pb systematics. Geochim. Cosmochim. Acta 50, 955–968.

Chen, J.H., Wasserburg, G.J., 1990. The isotopic composition of Ag in meteorites and the presence of ^{107}Ag in protoplanets. Geochim. Cosmochim. Acta 54, 1729–1743.

Connelly, J.N., Amelin, Y., Krot, A.N., Bizzarro, M., 2008. Chronology of the Solar System's oldest solids. Astrophys. J. 675, L121–L124.

Dodson, R.W., Forney, G.J., Swift, E.H., 1936. The extraction of ferric chloride from hydrochloric acid solutions by isopropyl ether. J. Amer. Chem. Soc. 58, 2573–2577.

Eisele, J., Abouchami, W., Galer, S.J.G., Hofmann, A.W., 2003. The 320 kyr Pb isotope evolution of Mauna Kea lavas recorded in the HSDP-2 drill core. Geochem. Geophys. Geosyst. 4, 8710. doi:10.1029/2002GC000339.

Gao, X., Thiemens, M.H., 1991. Systematic study of sulfur isotopic composition in iron meteorites and the occurrence of excess ^{33}S and ^{36}S. Geochim. Cosmochim. Acta 55, 2671–2679.

Göpel, C., Manhès, G., Allègre, C.J., 1985. U–Pb systematics in iron meteorites: uniformity of primordial lead. Geochim. Cosmochim. Acta 49, 1681–1695.

Haack, H., Scott, E.R.D., 1992. Asteroid core rystallization by inward dendritic growth. J. Geophys. Res. 97, 14,727–14,734.

Haack, H., Scott, E.R.D., Love, S.G., Brearley, A.J., McCoy, T.J., 1996. Thermal histories of IVA stony-iron and iron meteorites: evidence for asteroid fragmentation and reaccretion. Geochim. Cosmochim. Acta 60, 3103–3113.

Hevey, P.J., Sanders, I.S., 2006. A model for planetesimal meltdown by ^{26}Al and its implications for meteorite parent bodies. Meteoritics Planet. Sci. 41, 95–106.

Hoel, P.G., Port, S.C., Stone, C.J., 1971. Introduction to Probability Theory. Houghton Mifflin, Boston.

Holtstam, D., Broman, C., Söderhielm, J., Zetterqvist, A., 2003. First discovery of stishovite in an iron meteorite. Meteoritics Planet. Sci. 38, 1579–1583.

Horan, M.F., Smoliar, M.I., Walker, R.J., 1998. ^{182}W and $^{187}Re–^{187}Os$ systematics of iron meteorites: chronology for melting, differentiation, and crystallization in asteroids. Geochim. Cosmochim. Acta 62, 545–554.

Irisawa, K., Hirata, T., 2006. Tungsten isotopic analysis on six geochemical reference materials using multiple collector-ICP-mass spectrometry coupled with a rhenium-external correction technique. J. Anal. At. Spectrom. 21, 1387–1395.

Jacobsen, B., Yin, Q.-z., Moynier, F., Amelin, Y., Krot, A.N., Nagashima, K., Hutcheon, I.D., Palme, H., 2008. $^{26}Al–^{26}Mg$ and $^{207}Pb–^{206}Pb$ systematics of Allende CAIs: Canonical solar initial $^{26}Al/^{27}Al$ ratio reinstated. Earth Planet. Sci. Lett. 272, 353–364.

Kleine, T., Mezger, K., Palme, H., Scherer, E., Münker, C., 2005. Early core formation in asteroids and late accretion of chondrite parent bodies: evidence from $^{182}Hf–^{182}W$ in CAIs, metal-richchondrites, and iron meteorites. Geochim. Cosmochim. Acta 69, 5805–5818.

Lagerbäck, R., Wickman, F.E., 1997. A new iron meteorite from Muonionalusta, northernmost Sweden. GFF 119, 193–198.

Lavielle, B., Marti, K., Jeannot, J.P., Nishiizumi, K., Caffee, M., 1999. The $^{36}Cl–^{36}Ar–^{40}K–^{41}K$ records and cosmic ray production rates in iron meteorites. Earth Planet. Sci. Lett. 170, 93–104.

Lee, D.-C., 2005. Protracted core formation in asteroids: evidence from high precision W isotopic data. Earth Planet. Sci. Lett. 237, 21–32.

Lodders, K., 2003. Solar system abundances and condensation temperatures of the elements. Astrophys. J. 591, 1220–1247.

Ludwig, K., 2003. ISOPLOT: a geochronological toolkit for Microsoft Excel 3.00. Berkeley Geochronology Center Special Publication No. 4, 2455 Ridge Road, Berkeley CA 94709.

Markowski, A., Quitté, G., Halliday, A.N., Kleine, T., 2006. Tungsten isotopic compositions of iron meteorites: chronological constraints vs. cosmogenic effects. Earth Planet. Sci. Lett. 242, 1–15.

Moynier, F., Koeberl, C., Quitté, G., Telouk, P., 2009. A tungsten isotope approach to search for meteoritic components in terrestrial impact rocks. Earth Planet. Sci. Lett. 286, 35–40.

Myers, R.J., Metzler, D.E., 1950. The distribution of ferric iron between hydrochloric acid and isopropyl ether solutions. II. Polymerization of the iron in the ether phase, the effect of the acid concentration on the distribution, and the two-ether-phase region. J. Amer. Chem. Soc. 72, 3772–3776.

Nimmo, F., 2009. Energetics of asteroid dynamos and the role of compositional convection. Geophys. Res. Lett. 36. doi:10.1029/2009GL037997.

Patterson, C., 1956. Age of meteorites and the earth. Geochim. Cosmochim. Acta 10, 230–237.

Peale, S.J., Cassen, P., Reynolds, R.T., 1979. Melting of Io by tidal dissipation. Science 203, 892–894.

Qin, L., Dauphas, N., Wadhwa, M., Masarik, J., Janney, P.E., 2008. Rapid accretion and differentiation of iron meteorite parent bodies inferred from $^{182}Hf–^{182}W$ chronometry and thermal modeling. Earth Planet. Sci. Lett. 273, 94–104.

Rasmussen, K.L., Ulff-M¿ller, F., Haack, H., 1995. The thermal evolution of IVA iron meteorites: evidence from metallographic cooling rates. Geochim. Cosmochim. Acta 59, 3049–3059.

Sato, Y., Sugisawa, K., Aoki, D., Yamamura, T., 2005. Viscosities of FeNi, FeCo and NiCo binary melts. Meas. Sci. Technol. 16, 363–371.

Scherstén, A., Elliott, T., Hawkesworth, C., Russell, S., Masarik, J., 2006. Hf–W evidence for rapid differentiation of iron meteorite parent bodies. Earth Planet. Sci. Lett. 241, 530–542.

Schönbächler, M., Carlson, R.W., Horan, M.F., Mock, T.D., Hauri, E.H., 2008. Silver isotope variations in chondrites: volatile depletion and the initial ^{107}Pd abundance of the solar system. Geochim. Cosmochim. Acta 72, 5330–5341.

Segatz, M., Spohn, T., Ross, M.N., Schubert, G., 1988. Tidal dissipation, surface heat flow, and figure of viscoelastic models of Io. Icarus 75, 187–206.

Stacey, J.S., Kramers, J.D., 1975. Approximation of terrestrial lead isotope evolution by a two-stage model. Earth Planet. Sci. Lett. 26, 207–221.

Stirling, C.H., Halliday, A.N., Porcelli, D., 2005. In search of live ^{247}Cm in the early solar system. Geochim. Cosmochim. Acta 69, 1059–1071.

Stirling, C.H., Halliday, A.N., Potter, E.-K., Andersen, M.B., Zanda, B., 2006. A low initial abundance of ^{247}Cm in the early solar system and implications for r-process nucleosynthesis. Earth Planet. Sci. Lett. 251, 386–397.

Tatsumoto, M., Knight, R.J., Allègre, C.J., 1973. Time differences in the formation of meteorites as determined from the ratio of lead-207 to lead-206. Science 180, 1279–1283.

Tatsumoto, M., Unruh, D.M., Desborough, G.A., 1976. U–Th–Pb and Rb–Sr systematics of Allende and U–Th–Pb systematics of Orgueil. Geochim. Cosmochim. Acta 40, 617–634.

Teshima, J., Wasserburg, G.J., El Goresy, A., Chen, J.H., 1986. A comparative petrologic study of iron meteorites with 107 Ag* anomalies. Geochim. Cosmochim. Acta 50, 2073–2087.

Tilton, G., 1973. Isotopic lead ages of chondritic meteorites. Earth Planet. Sci. Lett. 19, 321–329.

Voshage, H., 1967. Bestrahlungsalter und Herkunft der Eisenmeteorite. Z. Naturforsch. 22a, 477–506.

Wadhwa, M., Bouvier, A., 2009. The age of the Solar System revisited. American Geophysical Union, Fall Meeting, San Francisco. EOS Trans. AGU 90. Abstract P12B-03.

Wang, P.-L., Rumble III, D., McCoy, T.J., 2004. Oxygen isotopic compositions of IVA iron meteorites: implications for the thermal evolution derived from in situ ultraviolet laser microprobe analyses. Geochim. Cosmochim. Acta 68, 1159–1171.

Wasson, J.T., Richardson, J.W., 2001. Fractionation trends among IVA iron meteorites: contrasts with IIIAB trends. Geochim. Cosmochim. Acta 65, 951–970.

Weyer, S., Anbar, A.D., Gerdes, A., Gordon, G.W., Algeo, T.J., Boyle, E.A., 2008. Natural fractionation of $^{238}U/^{235}U$. Geochim. Cosmochim. Acta 72, 345–359.

Wheeler, K.T., Walker, D., Fei, Y., Minarik, W.G., McDonough, W.F., 2006. Experimental partitioning of uranium between liquid iron sulde and liquid silicate: implications for radioactivity in the Earths core. Geochim. Cosmochim. Acta 70, 1537–1547.

Wyatt, M.C., 2008. Evolution of debris disks. Annu. Rev. Astron. Astrophys. 46, 339–383.

Yang, J., Goldstein, J.I., Scott, E.R.D., 2007. Iron meteorite evidence for early formation and catastrophic disruption of protoplanets. Nature 446, 888–891.

Yang, J., Goldstein, J.I., Scott, E.R.D., 2008. Metallographic cooling rates and origin of IVA iron meteorites. Geochim. Cosmochim. Acta 72, 3043–3061.